Experimental and theoretical rationalization of the growth mechanism of silicon quantum dots in non-stoichiometric SiN_x : role of chlorine in plasma enhanced chemical vapour deposition

2016 Nanotechnology 27 455703

(http://iopscience.iop.org/0957-4484/27/45/455703)

IOP Publishing Nanotechnology
Nanotechnology 27 (2016) 455703 (12pp) doi:10.1088/0957-4484/27/45/455703

Experimental and theoretical rationalization of the growth mechanism of silicon quantum dots in non-stoichiometric SiN_x: role of chlorine in plasma enhanced chemical vapour deposition

E Mon-Pérez[1], J Salazar[1], E Ramos[1], J Santoyo Salazar[2], A López Suárez[3], A Dutt[1], G Santana[1] and B Marel Monroy[1]

[1] Departamento de Materiales de Baja Dimensionalidad, Instituto de Investigaciones en Materiales, UNAM, Circuito Exterior s/n, C. U., A. P. 70-360, Coyoacán, C. P. 04510, México, D. F., Mexico
[2] Departamento de Física, CINVESTAV-IPN, A. P. 14-740, C. P. 07000, México, D. F., Mexico
[3] Departamento de Física Experimental, Instituto de Física, UNAM, Circuito Exterior s/n, C. U., A. P. 20-364, Coyoacán, C. P. 04510, México, D. F., Mexico

E-mail: marel@iim.unam.mx

Received 31 May 2016, revised 2 September 2016
Accepted for publication 9 September 2016
Published 3 October 2016

Abstract

Silicon quantum dots (Si-QDs) embedded in an insulator matrix are important from a technological and application point of view. Thus, being able to synthesize them *in situ* during the matrix growth process is technologically advantageous. The use of SiH_2Cl_2 as the silicon precursor in the plasma enhanced chemical vapour deposition (PECVD) process allows us to obtain Si-QDs without post-thermal annealing. Foremost in this work, is a theoretical rationalization of the mechanism responsible for Si-QD generation in a film including an analysis of the energy released by the extraction of HCl and the insertion of silylene species into the terminal surface bonds. From the results obtained using density functional theory (DFT), we propose an explanation of the mechanism responsible for the formation of Si-QDs in non-stoichiometric SiN_x starting from chlorinated precursors in a PECVD system. Micrograph images obtained through transmission electron microscopy confirmed the presence of Si-QDs, even in nitrogen-rich (N-rich) samples. The film stoichiometry was controlled by varying the growth parameters, in particular the NH_3/SiH_2Cl_2 ratio and hydrogen dilution. Experimental and theoretical results together show that using a PECVD system, along with chlorinated precursors it is possible to obtain Si-QDs at a low substrate temperature without annealing treatment. The optical property studies carried out in the present work highlight the prospects of these thin films for down shifting and as an antireflection coating in silicon solar cells.

Keywords: silicon nitride, nanoclusters, PECVD, DFT, reaction mechanism

(Some figures may appear in colour only in the online journal)

1 Introduction

Silicon nitride (SiN_x) is a material of great technological importance due to the combination of its chemical, electrical, mechanical and optical properties. In particular, in silicon solar cells, due to their anti-reflecting and passivating coating properties, are presently one of the most used materials [1, 2]. Due to the presence of small QDs embedded in the SiN_x

Table 1. Stoichiometry parameter, deposition parameters, and thickness of all studied samples.

Sample		Stoichiometry parameter (x)	NH_3 flow rate (sccm)	Flow ratio (R) NH_3/ SiH_2Cl_2	Flow rate H_2 (sccm)	Thickness (nm)
Si-rich	1	0.86	7.5	1.00	40	335.0 ± 27.6
	2	1.08	10	1.33		320.4 ± 10.8
	3	1.28	7.5	1.00	80	541.0 ± 5.6
N-rich	4	1.35	15	2.0	40	537.0 ± 0.7
	5	1.42	15		80	749.0 ± 3.6
	6	1.43	20	2.67		778.0 ± 11.4
	7	1.44	20		40	538.0 ± 3.6
	8	1.55	10	1.33	80	746.0 ± 0.6

matrix and their suitable optical properties, this material could also be used for the fabrication of third generation solar cells, where it would play an important role in enhancing the conversion in the blue region of the whole spectrum [3]. Furthermore, numerous applications in the market are based on the properties and quality of these films grown by various methods, which are finally determined by their film structure and stoichiometry.

Usually, Si-QDs are obtained from the use of silane as a precursor of Si [4, 5] and followed by high temperature post-annealing of a Si-rich SiN_x film at above 1000 °C [6, 7]. In already published reports, the formation of as-grown Si-QDs using chlorinated silanes at deposition temperatures lower than 350 °C has been shown [8–11]. It has been observed that the size dispersion, density and crystallinity of as-grown Si-QDs depends mainly on the type of precursor gases used during the plasma enhanced chemical vapour deposition (PECVD) process. However, there are rare reports that have analysed the growth mechanism of SiN_x films by PECVD using SiH_2Cl_2 and NH_3 as precursors [12]. There is even a recent study related to the theoretical explanation of the passivation of silicon quantum dots by halide atoms [13].

Up to now, theoretical reports have focused on the growth description of a stoichiometric SiN_x thin film, without mentioning the possible presence of non-stoichiometric defects that could induce the presence of Si–Si bonds [9–11]. On the other hand, these reports analysed the growth in a conventionally activated thermal CVD process. However, in this work, we will study in detail aspects of the PECVD process where there can be chemical reactions occurring out of thermodynamic equilibrium. Since electronic temperatures can typically attain 2000 K in these systems, many processes can be energetically favourable. Among all of the precursors used in the deposition process, atomic hydrogen (H_{at}) bombardment is expected to play a major role [14, 15]. Two approaches can be found in the literature: one that supports Si-QD generation in the gas phase in the plasma region [16, 17], and the second approach favours the growth of Si-QDs via gas–surface interactions [18].

Most of the theoretical analyses have been done in the gas phase. The most important considerations of the derived gaseous phase reactions are: (i) SiH_2Cl_2 can present a series of decomposition reactions, where the by-products can be the silylene species of the type R–Si–R'. Where, R and R' could be H or Cl atoms, with the elimination of H_2, HCl or Cl_2 [19]. (ii) In a silylene species, the Si atom has two unpaired electrons available that influence the overall reactivity of the group. Furthermore, if there are more Cl atoms available this could also affect the bonding probability of the Si atom [20]. (iii) The insertion–elimination reactions of the silylene species can be generated within the N–H bond of NH_3 [19, 21]. Among all of the surface reactions, the most important considerations are: (i) there exist reaction centres based on Si or N, where sets of reactions can be carried out that promote the film growth [19, 22]. (ii) Clusters of atoms are modelled to carry out the simulation process with different calculations of energies related to the various reaction processes [19, 23, 24].

In this work, we investigated the *in situ* generation mechanism of Si-QDs embedded in non-stoichiometric SiN_x thin films, for both cases, i.e. the silicon-rich ($SiN_{x<1.33}$) and the nitrogen-rich samples ($SiN_{x>1.33}$). Using transmission electron microscopy (TEM), we demonstrated the presence of small sized Si-QDs around 3–6 nm embedded in the SiN_x films. We propose that this occurs due to the insertion and elimination reactions of the silylene species (SiH_2, SiHCl, and $SiCl_2$) on the surface of the thin films. We believe that the chlorine chemistry is fundamental for the as-grown generation of Si-QDs, especially in the N-rich case. In general, the extraction of Cl on the surface in the form of HCl and the insertion of silylene species provokes local reaction and heating processes that help in the generation of QDs. It is noteworthy that other groups working with SiH_4 have not observed Si-QDs in nitrogen-rich samples [25]. Therefore, we propose an explanation of the experimental results together with theoretical calculations obtained from density functional theory (DFT) analysis for SiN_x thin films obtained by PECVD using SiH_2Cl_2 as a precursor. The DFT calculations were carried out simulating either a Si- or N-rich surface passivated with H or Cl atoms with a periodic model.

2 Experimental methods

The SiN_x thin films were deposited on high-resistivity n-type [1 0 0] monocrystalline silicon substrates using a conventional customized PECVD fabricated by INTERCOVAMEX SA de CV with direct coupling, parallel plates 150 cm^2 in

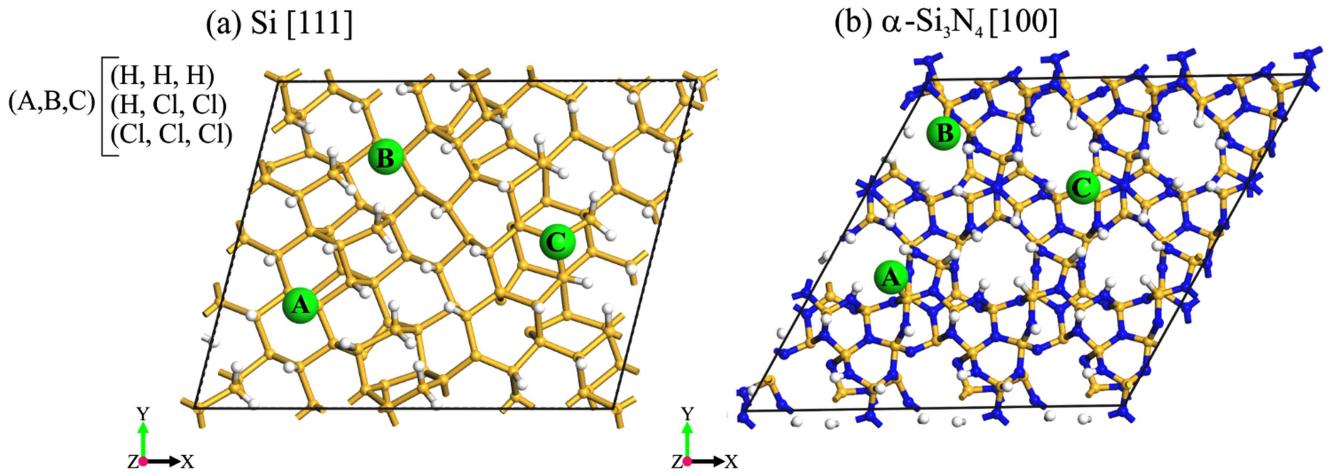

Scheme 1. Schematic representation for (a) the Si [111] surface and (b) the α-Si_3N_4 [100] surface. The different types of silylene react with N or Si on the surface. The surface termination and passivation could be due to H or Cl atoms, and is indicated by the investigated surface sites labelled as A, B and C.

area, 1.5 cm apart, activated by a 13.56 MHz radiofrequency (RF) signal. Before deposition, the silicon substrates were cleaned with a typical procedure and etched in a *p* solution (1:10:100; HF: HNO_3:H_2O) to clean the surface of the substrate. High purity SiH_2Cl_2, NH_3, H_2 and Ar were used as precursor gases. The SiH_2Cl_2 and Ar flow rates were fixed at 7.5 sccm and 50 sccm, respectively, while the NH_3/SiH_2Cl_2 flow ratio (*R*) and H_2 flow rate were varied as shown in table 1. In all cases, the substrate temperature, deposition time, the RF plasma power and the deposition pressure were fixed at 200 °C, 30 min, 30 W and 500 mTorr, respectively.

A Gaertner L117F Null Ellipsometer equipped with a He–Ne laser ($\lambda = 632.8$ nm) was used to determine the thickness and refractive index of the thin films. Table 1 summarizes the stoichiometry parameter, deposition parameters, and thickness of all studied samples.

The elemental composition profiles of the films were evaluated by Rutherford backscattering spectrometry (RBS). RBS measurements were carried out using a 3 MV Tandem accelerator (NEC 9SDH-2 Pelletron) at IF-UNAM, México. The backscattered ions were collected at a scattering angle of 167°. Analyses were performed using a collimated 3.045 MeV $^4He^+$ ion beam to get the atomic concentration of the samples. The elastic scattering resonance $^{16}O(\alpha, \alpha)\ ^{16}O$ at 3.045 MeV, which is 25 times larger than its corresponding Rutherford cross section, was used to obtain high sensitivity in the oxygen measurement. The SIMNRA code was used for the simulation and analysis of the RBS spectra. This analysis allowed us to quantify the atomic fraction of the elements present in the films. The hydrogen concentration of the samples was evaluated by Fourier transform infrared (FTIR) measurements, and this data was also used as input in the SIMNRA code.

The size and structure of the Si-QDs were confirmed by TEM images and selected area electron diffraction (SAED), respectively. The thin films of the samples were scratched from the surfaces and supported in Lacey Formvar stabilized with carbon copper grids, 400 mesh. Samples were observed

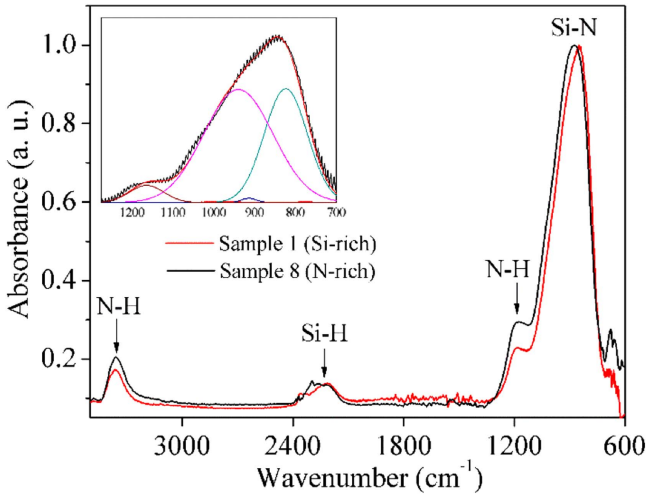

Figure 1. Representative FTIR spectra corresponding to sample 1 (Si-rich) and sample 8 (N-rich). The inset evidences the absence of the Si–O stretching mode after deconvolution of the spectra in the range 700–1300 cm^{-1}.

using TEM, JEOL (JEM-2010) with a LaB_6 filament with an acceleration voltage at 200 kV and wavelength of 0.0027 nm. The SAED images were obtained with a camera distance of 20 cm.

The chemical bonding structure of the films was analysed by using a FTIR spectrometer (Nicolet-560) in the range 400–4000 cm^{-1}.

3 Computational details

All calculations were carried out using Dmol3 [26, 27]. Electronic calculations were undertaken by applying a double numerical basis set. We used an orbital cut-off of 3.4 Ha. The exchange-correlation interaction was treated within the generalized gradient approximation with the revised functional parameterized by Perdew, Burke and Ernzerhof (PBE) [28].

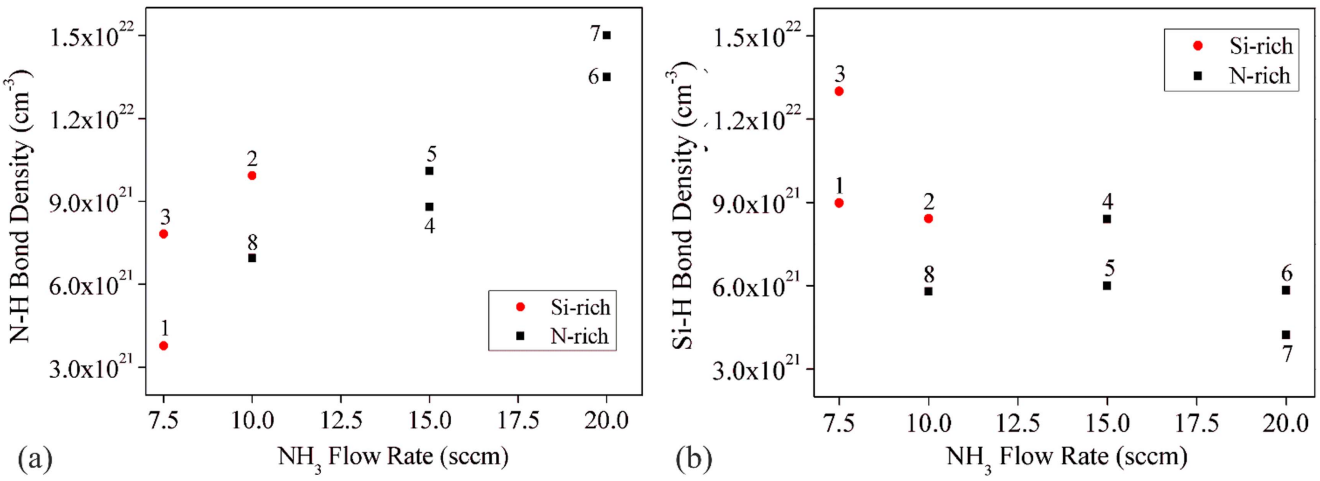

Figure 2. Hydrogen-related bond concentrations, (a) N–H bond density and (b) Si–H bond density, as a function of NH_3 flow rate.

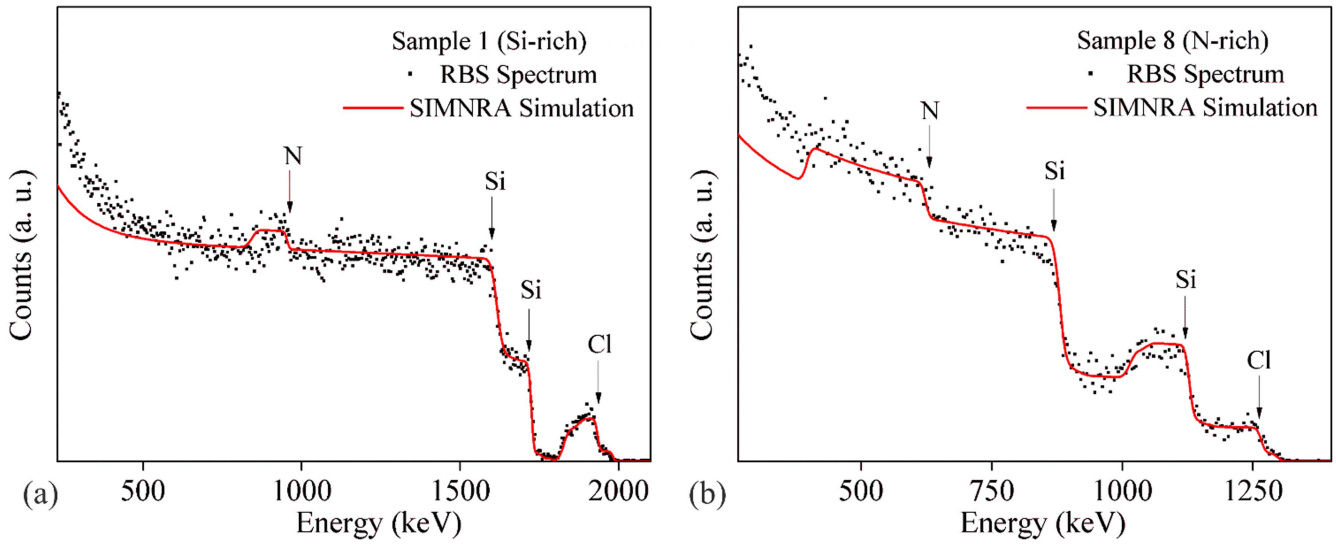

Figure 3. RBS spectra and SIMNRA simulations corresponding to as-deposited (a) sample 1 (Si-rich) and (b) sample 8 (N-rich). The arrows indicate the starting position of the Si, Cl and N elements.

Table 2. Atomic fraction of the elements Si, N and Cl (obtained by RBS) present in the films. The atomic fraction of H was obtained from the FTIR spectra shown in figure 1.

		Atomic fraction			
Sample		Si (%)	N (%)	Cl (%)	H (%)
Si-rich	1	35.0	30.0	10.0	25.0
	2	32.5	35.2	7.5	24.9
	3	25.0	32.0	8.9	34.1
N-rich	4	32.0	43.3	8.5	16.2
	5	25.0	35.6	7.5	31.9
	6	23.5	33.5	6.8	36.2
	7	28.0	40.2	7.5	24.3
	8	24.0	37.2	7.5	31.3

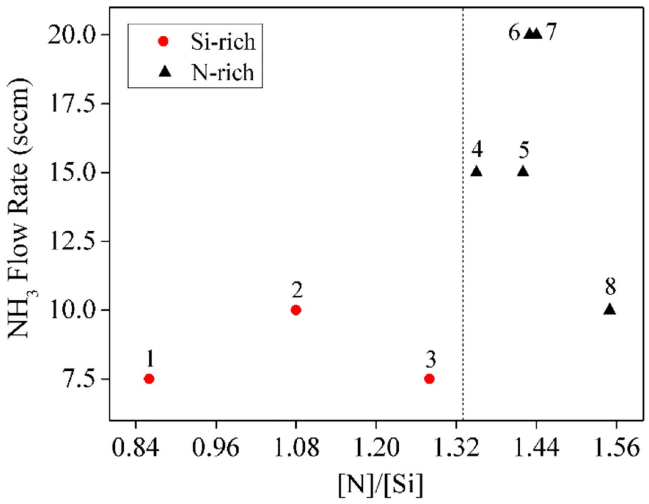

Figure 4. Graphical representation of the ammonia flow rate as a function of the stoichiometry of the thin films.

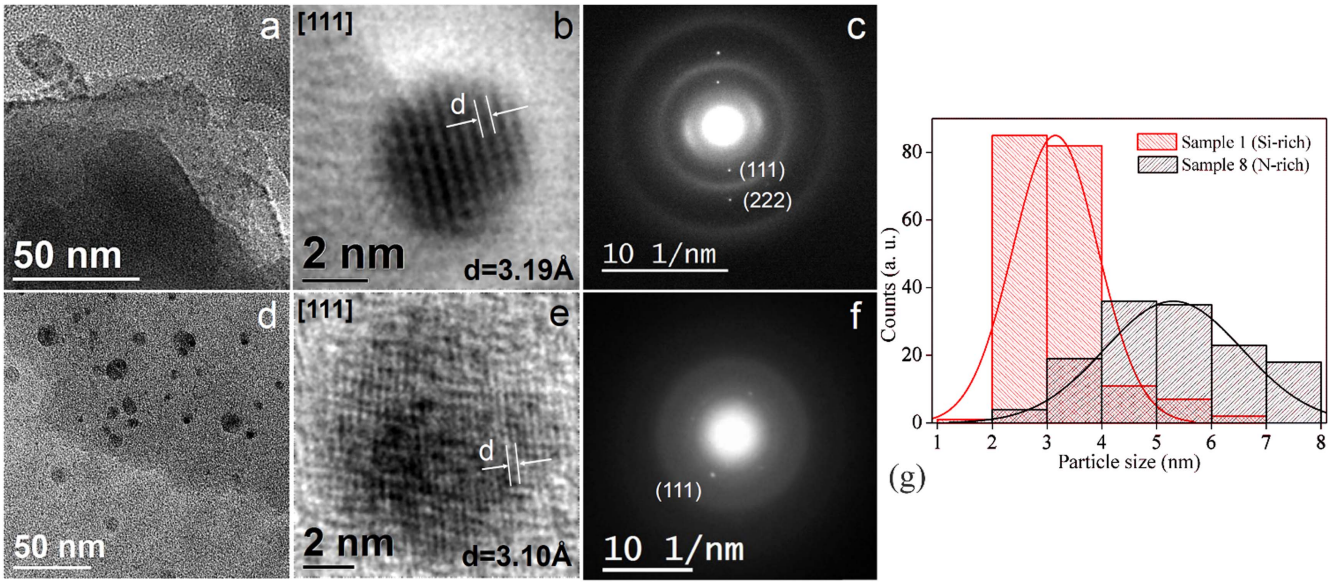

Figure 5. Global TEM micrograph of the Si-QDs embedded in the amorphous SiN_x matrix; (a) corresponds to sample 1 (Si-rich) and (d) sample 8 (N-rich). The images (b) and (e) show a zoom of a Si-QD of images (a) and (d), respectively. (c) and (f) represents the SAED of images (b) and (e), respectively, presenting the orientation of the crystalline planes in the Si-QD.

The convergence threshold for the self-consistent field, energy gradient and displacement was set to 1×10^{-5}, 2×10^{-3} Ha nm^{-1} and 5×10^{-3} nm, respectively, for all calculations. All surfaces were modelled using a supercell scheme described elsewhere [29], from a bulk structure for the crystalline silicon in the fcc [111] direction and the well-established crystalline phase of silicon nitride α-Si_3N_4 [30] in the [100] growth direction. The supercell presents 242 atoms ($a = b = 23.298$ Å and $c = 24.3247$ Å; $\alpha = \beta = \gamma = 90°$). Each surface was placed in a supercell that had at least 10 Å between periodic replicas in the c direction. This avoids spurious interactions between atoms belonging to vicinal cells due to the periodic boundary conditions imposed for the calculations. It is important to emphasize that our model envisions considering the gas–surface interactions by modelling the solid surface, which differs from previous theoretical works [17, 20, 24].

Scheme 1 shows the unit cells used for Si and α-Si_3N_4. These two surfaces were used in the model to represent Si-rich and N-rich environments, since we have a nanocomposite material consisting of Si-QDs embedded in an amorphous SiN_x matrix. The interaction between silylenes with the surface is stimulated by forming a bond between one of the Si or N atoms from the surface with the corresponding silylene.

The study of the energy released by the extraction of HCl from SiN_x and Si surfaces was performed by evaluating the surface energies of Si or α-Si_3N_4. This was done on the corresponding surface of the same system with a hole due to the absence of hydrogen in positions that could be related to the extraction process because of atomic bombardment. The same is shown schematically in scheme 1. We propose an explanation of the mechanism responsible for the formation of the Si-QD starting from NH_3/SiH_2Cl_2 precursors in PECVD systems.

4 Results and discussion

4.1 Chemical characterization

4.1.1 FTIR. The use of chlorinated precursors in the PECVD process can be a drawback for the chemical stability of the films, especially when taking into account the chlorine reactivity after ambient exposure. Stability is one of the most important parameters for the application in the photovoltaic devices industry. Excess of Cl incorporated into the thin films could cause degradation in the chemical stability due to the hydrolysis reactions that occur with moisture present in the environment to generate HCl or ammonia salts, promoting an oxidation process [12]. Stability was monitored by periodic FTIR measurements.

Figure 1 shows the representative as-grown FTIR spectra of the most Si-rich (sample with the highest atomic fraction of Cl) and N-rich SiN_x films, evidencing the sample's resistance to oxidation. All the spectra consisted mainly of one strong absorption band that corresponds to the Si–N stretching vibration around 860 cm^{-1}. As can be seen from figure 1, hydrogen is mainly bonded with nitrogen and silicon species at N–H bending (stretching) modes located at 1180 cm^{-1} (3360 cm^{-1}) and a Si–H stretching mode near 2220 cm^{-1}. In addition, the lack of a Si–O stretching mode around 1070 cm^{-1} was evident in all of the cases and confirms the stability and resistance to oxidation. The inset in figure 1 evidences the absence of the Si–O stretching mode after deconvolution of the spectra in the range 700–1300 cm^{-1}. This zone was deconvoluted in four peaks corresponding to different Si–N groups [31]. The same has been confirmed from the compositional results obtained using the RBS measurements (oxygen resonance) in figure 3.

The hydrogen bond density in the films (Si–H and N–H) as a function of NH_3 flow rate, were calculated from FTIR

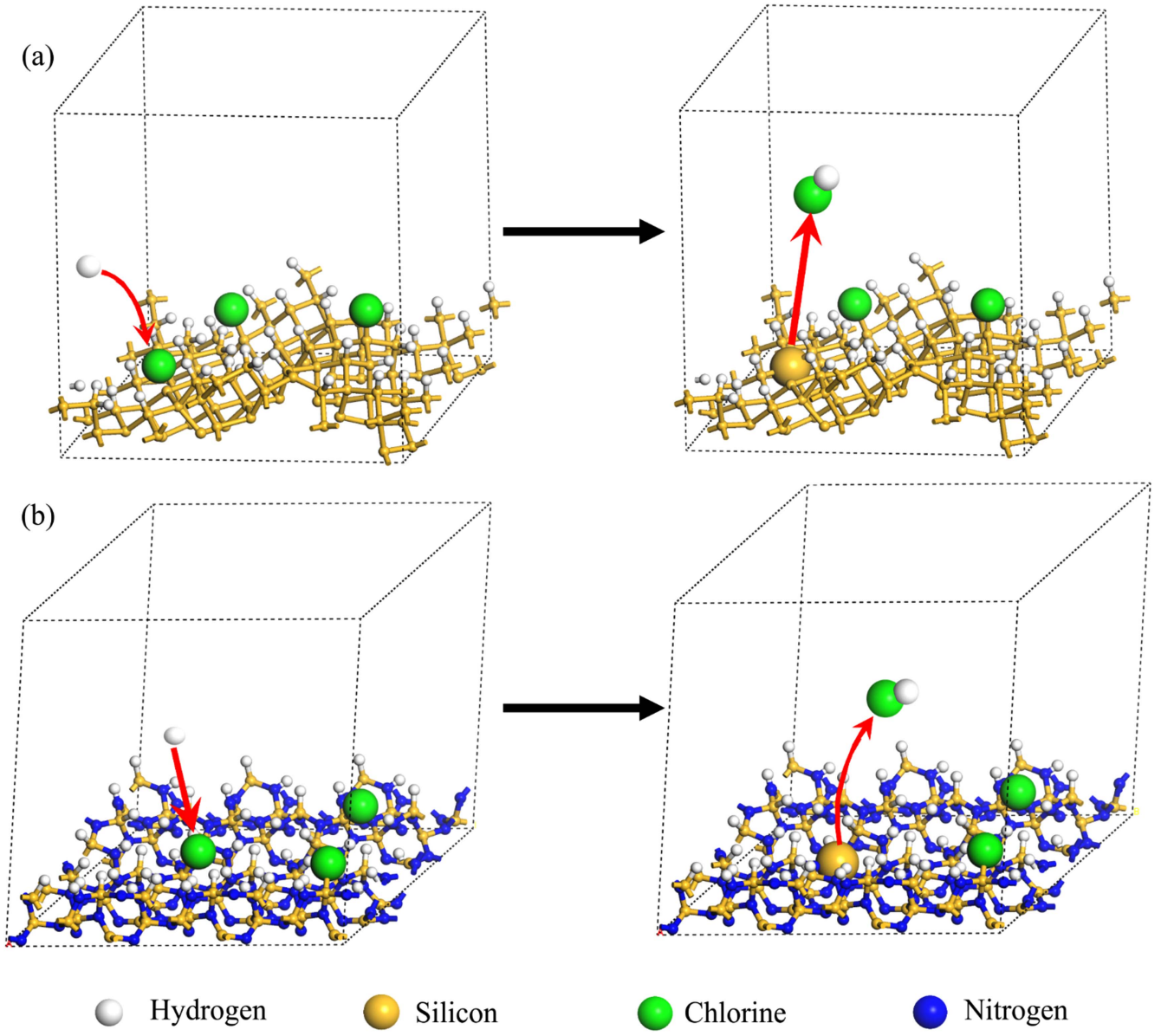

Scheme 2. Extraction reaction of chlorine from the (a) Si and (b) α-Si_3N_4 surfaces.

Table 3. Respective values of the exothermic reaction of HCl in SiN_x (a) Si-rich samples and (b) N-rich samples.

Cl atomic %	Stoichiometry	ΔE (kcal mol^{-1})
(a) **Reaction** H, Cl–[Si]Cl_y + H_{at} → hole–[Si]Cl_y + HCl		
4.2	$Si_{104}H_{46}Cl_2$	−27.44
6.2	$Si_{104}H_{45}Cl_3$	−31.66
(b) **Reaction** H, Cl–[Si–N]Cl_y + H_{at} → hole–[Si–N]Cl_y + HCl		
3.8	$Si_{79}N_{107}H_{51}Cl_2$	−0.16
5.7	$Si_{79}N_{107}H_{50}Cl_3$	−2.43

spectra using the following expression [32] and illustrated in figure 2

$$[C_1 - C_2] = \frac{\ln 10}{d} K_{[C_1-C_2]} \int A(w)\,\mathrm{d}w \qquad (1)$$

where, $[C_1 - C_2]$ corresponds to the hydrogen-related bond concentrations, d is the sample thickness in cm, $A(w)$ is the absorbance of each band as function of the wavenumber w ($\int \alpha(w)\mathrm{d}w$ is the normalized absorption area of the band and $\alpha = \frac{\ln 10}{d} A$ is the absorption coefficient). $K_{[C_1-C_2]}$ is an empirical constant with values as: $K_{[\mathrm{Si-H}]} = 7.1 \times 10^{16}$ cm^{-1} and $K_{[\mathrm{N-H}]} = 8.2 \times 10^{16}$ cm^{-1} [32].

Table 4. Calculated reaction energy of the inserted silylene species in Si-rich surfaces, where we presume the existence of several Si–Si defects.

Reactions H (Cl)–[Si]Cl_y + Y → hole–[Si]Cl_y*n* hole–[Si]Cl_y + Y → Y–H[Si]Cl_y Y = silylene (SiH_2, SiHCl, $SiCl_2$)			
% Atomic Cl	Hole formation	Silylene (Y)	ΔE (kcal mol^{-1})
4.2% $Si_{79}H_{46}Cl_2$	Cl extraction from the Si–Cl bond	SiH_2	−49.38
		SiHCl	−42.77
		$SiCl_2$	−37.68
	H extraction from the Si–H bond	SiH_2	−49.14
		SiHCl	−41.58
		$SiCl_2$	−36.62
6.2% $Si_{79}H_{46}Cl_3$	Cl extraction from the Si–Cl bond	SiH_2	−52,64
		SiHCl	−36,06
		$SiCl_2$	−27,71
	H extraction from the Si–H bond	SiH_2	−46,83
		SiHCl	−39,86
		$SiCl_2$	−33,09

The atomic fraction of the total hydrogen present was determined by using the relation (2) [33], and obtained values are shown in table 2

$$\text{Fraction H} = \frac{[\text{Si} - \text{H}] + [\text{N} - \text{H}]}{[\text{Si} - \text{H}] + [\text{N} - \text{H}] + [\text{Si} - \text{N}]} \quad (2)$$

where $K_{[\text{Si}-\text{N}]} = 1.82 \times 10^{16}\,\text{cm}^{-1}$ [29].

4.1.2 RBS. RBS was used to analyse the elemental composition profiles of the samples. Figure 3 illustrates the characteristic RBS spectra of the samples 1 (Si-rich) and 8 (N-rich). The simulation results attained using SIMNRA are also displayed, taking into account the calculated hydrogen fraction (table 2) from FTIR spectra for each sample. The chi-square (χ^2, defined in the usual way as a weighted distance between the experimental data and proposed theoretical function) calculated for each sample ($\chi^2 = 1.7$ for sample 1 and $\chi^2 = 7.1$ for sample 8) assure the good adjustment made to the experimental data. As evidenced in figure 3(a), the sample with higher Cl content (sample 1) shows the absence of oxygen and confirms the results obtained from FTIR spectroscopy in figure 1. The atomic fraction of all the elements present in the films shown in figure 3 is also shown in table 2.

4.1.3 Stoichiometry. The ideal value of the ratio x for a stoichiometric SiN_x sample is 1.33. The stoichiometry parameter of each sample is presented in table 1. On the basis of the results obtained, they were further classified in between the two different compositions, Si-rich ($SiN_{x<1.33}$) and N-rich ($SiN_{x>1.33}$), where $\left(x = \frac{\text{N}}{\text{Si}}\right)$ was determined from the atomic fractions obtained by RBS in table 2. Figure 4 shows the stoichiometry of the SiN_x films, where two different regions can be seen, which permits us to classify Si-rich and N-rich samples.

4.2 Microstructural characterization

4.2.1 TEM. The TEM images displayed in figure 5 evidence the presence of Si-QDs embedded in the amorphous matrix of SiN_x for both Si-rich and N-rich samples. In addition, the size distribution and density of the Si-QDs in the films was obtained using the Digital Micrograph 3.7.0, software by Gatan, Inc. USA.

4.2.2 In situ formation of Si-QDs in Si-rich areas. H_{at} present in the plasma deposition process plays a key role in the growth of Si-QDs/SiN_x, as it helps to extract the Cl on the superficial surface of the thin film (scheme 2) forming a HCl bond (highly exothermic reaction [19, 23, 24]), and the respective values are shown in tables 3(a) and (b). ΔE corresponds to the change in the reaction energy, which could be exothermic or endothermic in nature.

In addition, there is also a major probability that H_{at} could also break the weaker bonds present in the thin film, either in the surface or in the bulk, due to the kinetic energy acquired during the plasma process, which can be up to 70 eV (~1614 kcal mol^{-1}) [34].

Furthermore, depending on the energy attained, these bonds could be formed on the surface or in the bulk of the thin film. Due to the surface reactions with H_{at}, there is the presence of free dangling bonds, where there is a probability for the insertion of silylene species as mentioned in table 4. However, H_{at} could also be incorporated into the thin film during the reaction process. In this case, N-rich samples have major incorporation of H_{at}, due to the greater dilution of H_2 employed during the deposition process (double with respect to Si-rich, as can be seen in table 1). It is important to mention that the total concentration of hydrogen in the chamber is not only from the source of H_2 but also from the source of NH_3,

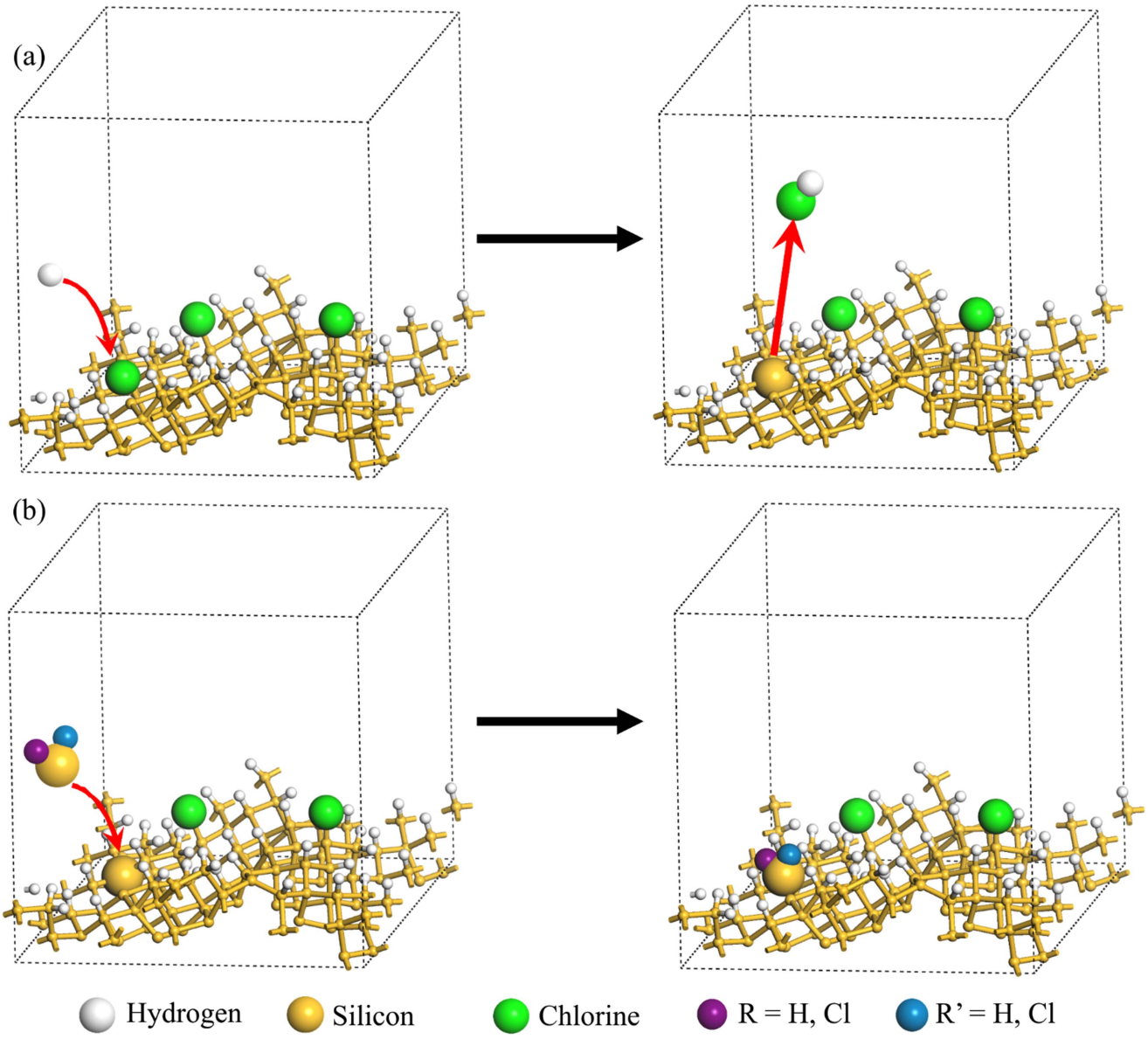

Scheme 3. Silylene insertion reactions in Si-rich surfaces, (a) HCl extraction and (b) silylene insertion in the reaction site.

which is rich in hydrogen. Hence, the greater dilution of H_2 (80 sccm) in the deposition of N-rich thin films generates a vast number of reaction centres due to the higher Cl extraction in comparison to Si-rich samples grown with a lesser dilution of hydrogen (40 sccm). This explains the higher Si-QD density observed by TEM in N-rich samples (figure 5).

As mentioned in an earlier report [35] there is dissociation energy of the most probable bonds to be broken (Si–H, N–H, and Si–Si) during the reaction process. Thus, breaking the Si–H and Si–Si bonds promotes the formation of reaction centres that further enhances the growth of the Si-QDs, whereas dissociation of N–H bond endorses the matrix growth. From the TEM analysis, the average size and density are of the order of 3.15 ± 0.78 nm and 2.89×10^{11} Si-QDs/cm^2, respectively, for the Si-rich thin films. Insertion of silylene species into Si–H, Si–Cl and Si–Si bonds can generate non-stoichiometric defects of the type Si–Si, as can be seen in scheme 3. Thus, it is expected that favoured insertion of the silylene species (exothermic reactions around 40–50 Kcal mol^{-1}) could encourage the nucleation process, which can further increase the average size of Si-QDs (figure 5(g)). According to the theoretical calculations obtained in this work, the insertion of silylenes on the superficial Si–Cl and Si–H bonds generates Si–Si bonds, which are the most favourable and exothermic reactions in all cases (table 4). Consequently of the exothermic reactions that could induce a local heating process in the thin film, the crystallinity of Si-QDs is enhanced, as evidenced by figure 5(b) and the SAED images in figure 5(c).

4.2.3 In situ formation of Si-QDs in N-rich areas. In areas where the matrix grows, i.e. areas with predominant N content in the film, the an insertion of silylene type in a Si–Cl on the surface or in the bulk are typical reactions

Table 5. Calculated reaction energy of the silylene insertion in N-rich surfaces.

Reactions H (Cl)–[Si–N]Cl_y + Y → hole–[Si–N]Cl_y hole–[Si–N]Cl_y + *Y* → *Y*–[Si–N]Cl_y Y = silylene (SiH_2, SiHCl, $SiCl_2$)			
Cl atomic %	Hole formation	Silylene (*Y*)	ΔE (kcal mol^{-1})
3.8% $Si_{79}N_{107}H_{51}Cl_2$	Cl extraction from the Si–Cl bond	SiH_2	3371.43
		SiHCl	3120.96
		$SiCl_2$	3379.03
	H extraction from the N–H bond	SiH_2	−52.78
		SiHCl	−47.86
		$SiCl_2$	−56.93
	H extraction from the Si–H bond	SiH_2	−49,44
		SiHCl	−44,21
		$SiCl_2$	−39,02
5.7 % $Si_{79}N_{107}H_{51}Cl_3$	Cl extraction from the Si–Cl bond	SiH_2	3398,16
		SiHCl	3401,94
		$SiCl_2$	3406,47
	H extraction from the N–H bond	SiH_2	−43,79
		SiHCl	−40,57
		$SiCl_2$	−38,07
	H extraction from the Si–H bond	SiH_2	−44,94
		SiHCl	−40,70
		$SiCl_2$	−36,42

that require much energy to take place (around 3000 kcal mol^{-1}, table 5). Hence, this type of bond effectively limits the size of the Si-QDs and also acts as a terminal bond. This behaviour is different from the one in Si-rich areas as discussed earlier. In this case, the Si-QD growth mainly occurs through silylene insertion into Si–H bonds, whereas in Si-rich areas this is favourable for all Si–H, Si–Cl and Si–Si bonds. For the N-rich thin films, using TEM analysis the average size and density are found to be of the order of 5.31 ± 1.26 nm and 2.47 × 10^{11} Si-QDs/cm^2, respectively. In this particular situation, the predominance of the N–H bond in comparison to Si–H causes the enrichment of nitrogen in the thin film. In this circumstance, one would expect that the film did not show any increase in the density of Si-QDs, however, the size of the QDs is bigger, as shown in figure 5(d). As mentioned previously, in the case of Si-rich films, calculations indicate that the insertion reactions of silylene species in the Si–H and N–H bonds are more favourable and exothermic as compared to the reaction of the Si–Cl bond. Since these reactions are exothermic, the conclusion, in N-rich films, is that the Si-QDs are crystalline in nature and the same us confirmed by tge SAED pattern in figure 5(f). By having a higher content of N–H bonds in the thin film, the probability of generating Si–N, is higher due to the insertion of silylene species, promoting the matrix growth. However, due to the greater dilution of hydrogen during the deposition process, there exists more probability of breaking the existing Si–H and Si–Si bonds. Therefore, numerous reaction centres are generated for the insertion of silylene species. Thus, due to the greater amount of dangling bonds, if two or more reaction centres are close to each other, this would result in agglomeration and, hence, in the overall increase in the size of the Si-QDs. Therefore, the growth of Si-QDs in N-rich thin films can occur in two different ways. The first route is the breaking of Si–H bonds due to the bombardment of sufficient H_{at} on the surface and also within the Si-QD, as shown in scheme 4. The other route is initiated by the breakage of the bulk Si–Si bond to insert the silylene species and generate non-stoichiometric defects of the type Si–Si. This generates many reaction centres and also increases the possibility of their agglomeration, which finally results in an overall increment in Si-QD size.

4.3 Optical characterization

The refractive index as a function of NH_3 flow rate is presented in figure 6. The film termed as the richest in Si, sample 1, shows a refractive index near to the ideal stoichiometric ($n_{Si_3N_4}$ = 2.02). In the films defined as N-rich samples, the refractive index shows a decrement as a result of the N and/or H increase, when the NH_3 flow rate or hydrogen dilution were increased. It is important to mention that the relation of refractive index to the thin film deposited (Si- or N-rich) is not direct. It depends on the concentration and arrangement of the structure of the resulting thin films formed. As can be seen from table 2, variation in the Cl and H_2 concentrations can be seen and this results in differences in the overall structure formation of the thin film, which could change the refractive index value as seen in figure 6.

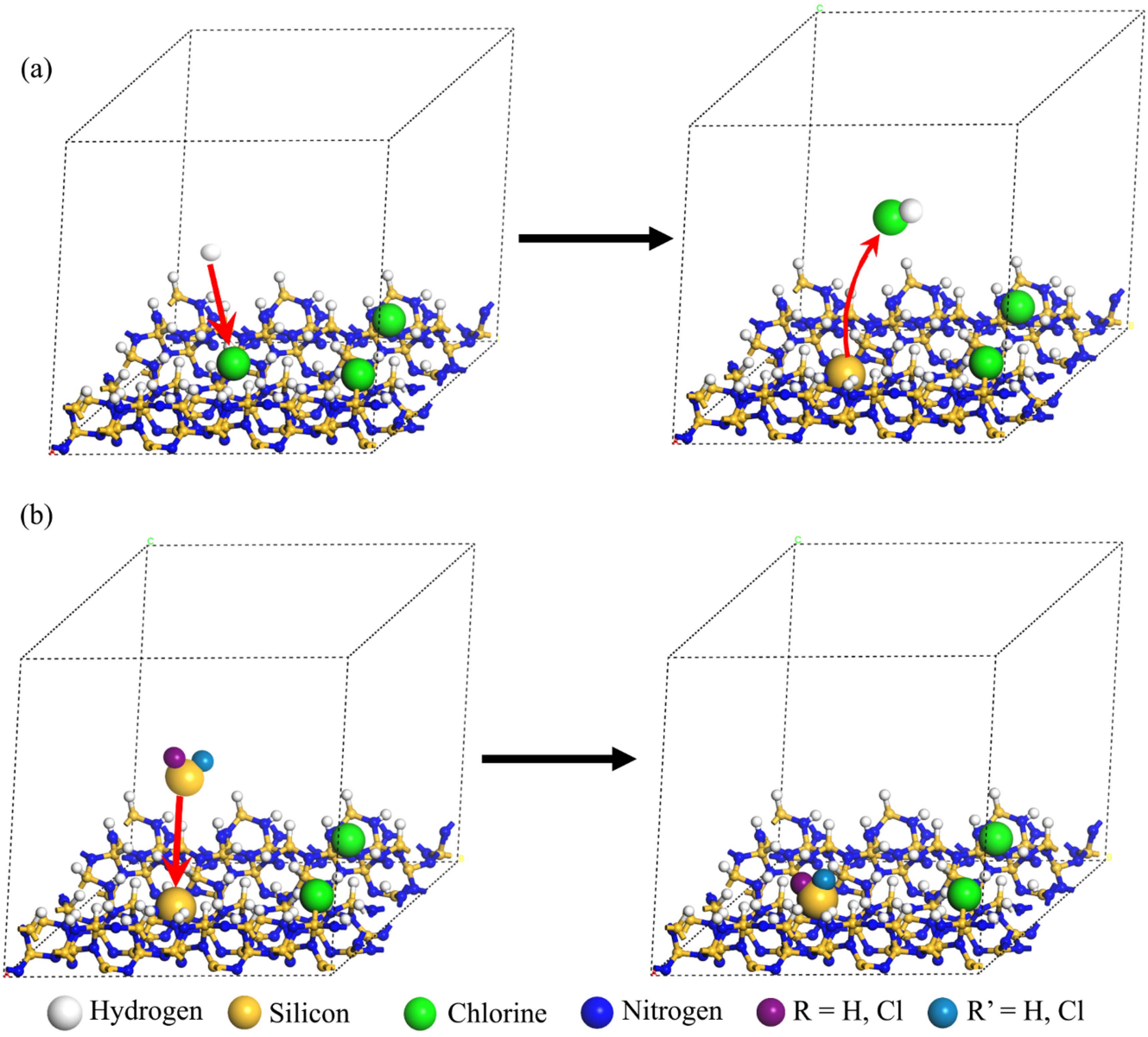

Scheme 4. Silylene insertion reactions in N-rich surfaces, (a) HCl extraction and (b) silylene insertion in the reaction site.

UV-excitation on selected samples, figure 7, presented a bright white photoluminescence spectra at room temperature (with the naked eye in the lighted room) and the emission was consistent with the quantum confinement effect model in Si-QDs [9, 10, 12] observed from QDs in figure 5. Since we obtain a broad emission in all the visible range, this sample would be a very good candidate for down shifting applications and antireflection coating in silicon-based solar cells.

As can be seen from figure 7, the Si-rich sample showed luminescence in the blue region whereas the N-rich sample showed orange-red emission. This can be explained by the TEM image in figure 5. For the Si-rich sample, there is the presence of particles in the regime of 2–3 nm and that particular distribution helps having an emission in the blue region. However, for both of the conditions (silicon-rich ($SiN_{x<1.33}$)) and nitrogen-rich ($SiN_{x>1.33}$) the majority of the samples are N-rich as observed from the figure 4. This particular condition helps in the improved passivation of the Si-QDs embedded in the matrix and, hence, helps in the bright and stable emission in the visible region. On the other hand, for both of the cases one cannot neglect the presence of a wide distribution of QDs (figure 5(g)), which could provoke emission with a broad peak.

Figure 8 shows the reflectance spectra of the Si-rich and N-rich samples. From the spectra it can be observed that the Si-rich sample, with a higher value of refractive index, shows the minimum total reflection, whereas for N-rich sample, with refractive index lower than 1.8, shows higher reflection. It can also be observed from the curves that the average reflection is much higher for the N-rich sample. The Si-rich sample, due to its refraction index close to the ideal values, can be used as antireflection coating in the case of

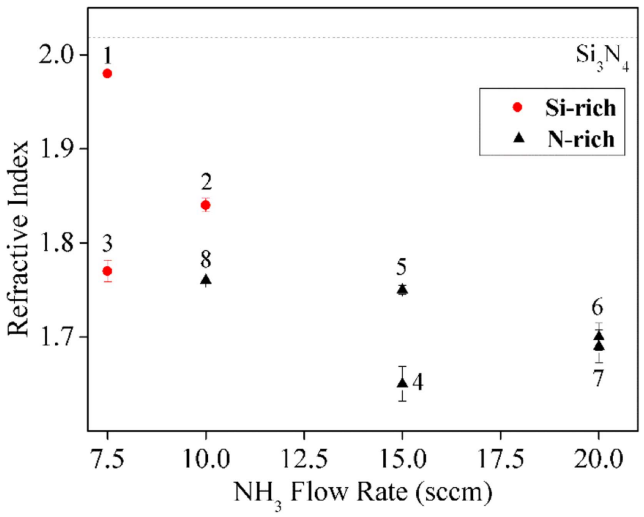

Figure 6. The refractive index of SiN_x thin films as a function of NH_3 flow rate.

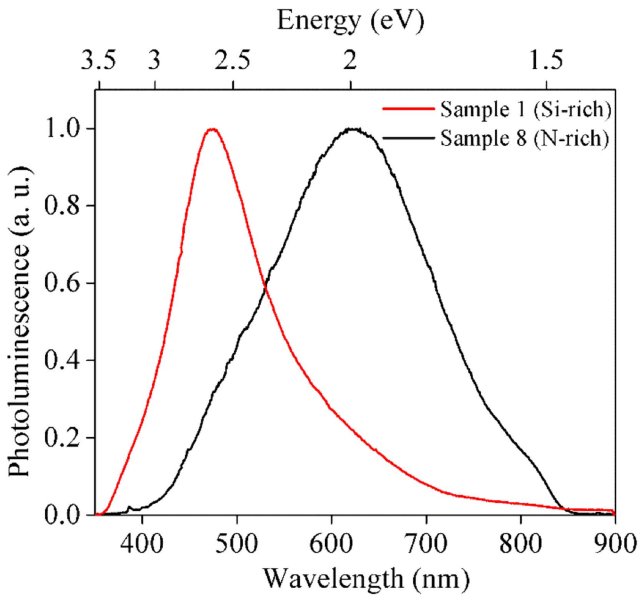

Figure 7. Visible photoluminescence spectra of Si-rich (sample 1) and N-rich (sample 8) films when excited with a He-Cd laser at room temperature.

silicon solar cells (figure 6). In a nutshell, all of the results obtained for the Si-rich sample show that it is appropriate for down shifting in third generation solar cells.

5 Conclusions

In summary, the *in situ* formation of crystalline Si-QDs embedded in an amorphous matrix of non-stoichiometric SiN_x, using SiH_2Cl_2, was demonstrated, irrespective of the final stoichiometry of the thin film (Si-rich or N-rich). The chlorine chemistry introduced by the silicon precursor is fundamental for the as-grown generation of Si-QDs, even in N-rich films. Increasing the hydrogen dilution during the

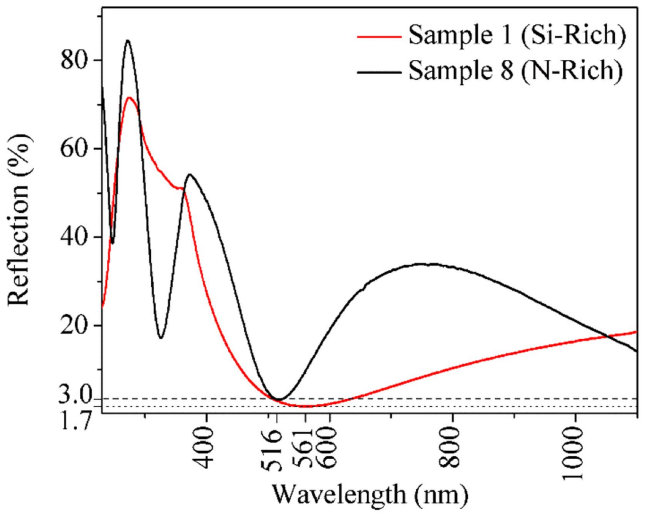

Figure 8. Reflectance spectra of the Si-rich and N-rich samples.

deposition process implies an increment in the H_{at} bombardment, which promotes the creation of more reaction centres for the insertion of the silylene species. In the case of N-rich thin films, the Si-QD growth occurs by the breaking of Si–H bonds due to the bombardment of sufficient H_{at} on the surface and also within the Si-QD. Moreover, by breaking the bulk Si–Si bond allows the insertion of the silylene species and the generation of non-stoichiometric defects of the type Si–Si. As a result of these insertion–elimination reactions, there is the possibility of agglomeration, resulting in an overall increment in Si-QDs size. In the case of Si-rich thin films the insertion of silylene species into Si–H, Si–Cl and Si–Si bonds generates the formation of non-stoichiometric defects of the type Si–Si. The theoretical studies reported in this work reinforces the development of Si-QDs embedded in an amorphous matrix starting from the gas–surface interaction. Further, this could help to achieve the repeatability of the film properties for large scale industrial production. Finally, depending on the tuneable nature of the refractive index and photoluminescence obtained in this work, the thin films could be used as a good antireflection coating as well as for down shifting in silicon-based solar cells.

Acknowledgments

The authors acknowledge financial support for this project from DGAPA-UNAM PAPIIT Projects IN100216, IN108215 and IN100914, CONACYT Project 179632 and SENER-CONACYT Project 151076. E Mon-Pérez is grateful for CONACYT scholarship 517361.

References

[1] Nagel H, Aberle A G and Hezel R 1999 Optimised antireflection coatings for planar silicon solar cells using remote PECVD silicon nitride and porous silicon dioxide *Prog. Photovoltaics Res. Appl.* **7** 245–60

[2] Rahman A *et al* 2015 Sub-50 nm self-assembled nanotextures for enhanced broadband antireflection in silicon solar cells *Nat. Commun.* **6** 5963

[3] Cho E C *et al* 2007 Silicon quantum dots in a dielectric matrix for all-silicon tandem solar cells *Adv. Optoelectron.* **2007**

[4] Kim T Y *et al* 2004 Quantum confinement effect of silicon nanocrystals *in situ* grown in silicon nitride films *Appl. Phys. Lett.* **85** 5355–7

[5] Wang Y *et al* 2005 Visible photoluminescence of Si clusters embedded in silicon nitride films by plasma-enhanced chemical vapor deposition *Physica* E **27** 284–9

[6] Carrada M *et al* 2008 Structural and optical properties of high density Si-QDs synthesized in SiNx:H by remote PECVD and annealing *Mater. Sci. Eng.* B **147** 218–21

[7] Esposito E M, Mercaldo L V, Veneri P D, Lancellotti L and Privato C 2010 Annealing effects on PECVD-grown Si rich aSiNx thin films *Energy Procedia* **2** 159–64

[8] Molinari M, Rinnert H and Vergnat M 2003 Correlation between structure and photoluminescence in amorphous hydrogenated silicon nitride alloys *Physica* E **16** 445–9

[9] Monroy B M *et al* 2009 Photoluminescence of as-grown silicon nanocrystals embedded in silicon nitride: influence of atomic hydrogen abundance *J. Nanosci. Nanotechnol.* **9** 2902–9

[10] Benami A *et al* 2007 Strong white and blue photoluminescence from silicon nanocrystals in SiN_x grown by remote PECVD using $SiCl_4/NH_3$ *Nanotechnology* **18** 155704–9

[11] Shirai H, Fujimura Y and Jung S 2002 Formation of nanocrystalline silicon dots from chlorinated materials by RF plasma-enhanced chemical vapor deposition *Thin Solid Films* **407** 12–7

[12] Monroy B M *et al* 2006 Photoluminescence properties of SiN_x/Si amorphous multilayer structures grown by plasma-enhanced chemical vapor deposition *J. Lumin.* **121** 349–52

[13] Ramos E *et al* 2012 Theoretical study of the electronic properties of silicon nanocrystals partially passivated with Cl and F *J. Phys. Chem.* C **36** 12427–31

[14] Shirai H, Hanna J-i and Shimizu I 1991 Role of atomic hydrogen during growth of hydrogenated amorphous silicon in the 'chemical annealing' *Jpn. J. Appl. Phys.* **30** 679–82

[15] Zecho T, Brandner B D, Biener J and Küppers J 2001 UHV study of hydrogen atom induced etching of amorphous hydrogenated silicon thin films *J. Phys. Chem.* B **105** 3502–9

[16] Bao J L and Truhl D G 2016 Silane-initiated nucleation in chemically active plasmas: validation of density functional, mechanisms, and pressure-dependent variational transition state calculations *Phys. Chem Chem. Phys.* **18** 10097

[17] Roca i Cabarrocas P, Chaabane N, Kharchenko A V and Tchakarov S 2004 Polymorphous silicon thin films produced in dusty plasmas: application to solar cells *Plasma Phys. Control. Fusion* **46** B235–43

[18] Bruneau B, Wang J, Dornstetter J C and Johnson. E V 2014 Growth mechanisms study of microcrystalline silicon deposited by SiH_4/H_2 plasma using tailored voltage waveforms *J. Appl. Phys.* **115** 084901

[19] Koseki S and Ishitani A 1992 Theoretical study on silicon-nitride film growth: *ab initio* molecular orbital calculations *J. Appl. Phys.* **72** 5808

[20] Jenkins R L, Vanderwielen A J, Ruis S P, Gird S R and Ring M A 1973 Pyrolysis of halodisilanes and the formation and insertion reactions of chlorosilylene and fluorosilylene pyrolysis of halodisilanes *Inorg. Chem.* **12** 2968–72

[21] Koseki S, Ishitani A and Fujimura Y 1997 Theoretical investigation on silicon-nitride film growth: statistical approach *Jpn. J. Appl. Phys.* **36** 6518–22

[22] Korkin A 1999 On the mechanism of silicon nitride chemical vapor deposition from dichlorosilane and ammonia *J. Electrochem. Soc.* **146** 4203

[23] Bagatur'yants A A *et al* 2000 Atomistic modeling of chemical vapor deposition: silicon nitride CVD from dichlorosilane and ammonia *Mater. Sci. Semicond. Process.* **3** 23–9

[24] Bagatur A A *et al* 2001 Silicon nitride chemical vapor deposition from dichlorosilane and ammonia: theoretical study of surface structures and reaction mechanism *Surf. Sci.* **486** 213–25

[25] Kistner J, Chen X, Weng Y, Strunk H P, Schubert M B and Werner J H 2011 Photoluminescence from silicon nitride no quantum effect *J. App. Phys.* **110** 023520

[26] Delley B 1990 An all-electron numerical method for solving the local density functional for polyatomic molecules *J. Chem. Phys.* **92** 508–17

[27] Delley B 2000 From molecules to solids with the DMol3 approach *J. Chem. Phys.* **113** 7756–64

[28] Hammer B, Hansen L and Nørskov J 1999 Improved adsorption energetics within density-functional theory using revised Perdew-Burke-Ernzerhof functionals *Phys. Rev.* B **59** 7413–21

[29] Trejo A, Calvino M, Ramos E and Cruz-Irisson M 2012 Computational simulation of the effects of oxygen on the electronic states of hydrogenated 3C-porous SiC *Nanoscale Res. Lett.* **7** 471

[30] Yashima M, Ando Y and Tabira Y 2007 Crystal structure and electron density of alpha-silicon nitride: experimental and theoretical evidence for the covalent bonding and charge transfer *J. Phys. Chem.* B **111** 3609–13

[31] Xu X, He Q, Fan T, Jiang Y, Huang L, Ao T and Ma C 2013 Hard and relaxed a-SiNxHy films prepared by PECVD: structure analysis and formation mechanism *Appl. Surf. Sci.* **264** 823–31

[32] Lanford W A and Rand M J 1978 The hydrogen content of plasma-deposited silicon nitride *J. Appl. Phys.* **49** 2473–7

[33] Weeber A W, Rieffe H C, Romijn I G, Sinke W C and Soppe W J 2005 The fundamental properties of SiN_x:H that determine its passivating qualities *Photovoltaic Specialists Conf. 2005: Conf. Record of the Thirty-first IEEE* pp 1043–6

[34] Yin Z and Smith F W 1990 Optical dielectric function and infrared absorption of hydrogenated amorphous silicon nitride films: experimental results and effective-medium-approximation analysis *Phys. Rev.* B **42** 3666–75

[35] Cottrell T L 1958 The strengths of chemical bonds *Properies of Atoms, Radicals and Bonds* 2nd edn (London: Butterworth) pp 41–53